Auger electron spectroscopy and work function characterization of oxygen adsorption on Ba-covered Ni(110)

2003 J. Phys.: Condens. Matter 15 8195

(http://iopscience.iop.org/0953-8984/15/47/022)

INSTITUTE OF PHYSICS PUBLISHING JOURNAL OF PHYSICS: CONDENSED MATTER

J. Phys.: Condens. Matter **15** (2003) 8195–8206 PII: S0953-8984(03)65151-9

Auger electron spectroscopy and work function characterization of oxygen adsorption on Ba-covered Ni(110)

D Vlachos[1], **N Panagiotides and S D Foulias**

Department of Physics, University of Ioannina, PO Box 1186, GR-451 10 Ioannina, Greece

E-mail: dvlachos@cc.uoi.gr

Received 20 June 2003, in final form 7 October 2003
Published 14 November 2003
Online at stacks.iop.org/JPhysCM/15/8195

Abstract

The adsorption of oxygen on a Ba-covered Ni(110) surface has been investigated mainly by Auger electron spectroscopy (AES) and work function (WF) measurements. Low energy AES lines indicate that O interacts with Ba and Ni as well. Both Ba–O and Ni–O interactions take place simultaneously on the surface, progressively leading to BaO and NiO formation. Ba enhances the oxidation of the substrate due to the higher sticking coefficient of O on the Ba/Ni surface. The oxygen interacts with the nickel substrate even at high adsorbate coverage, incorporating under the Ba layer. A part of the Ba adatoms remains non-oxidized even at a high O exposure.

1. Introduction

The oxidation of alkaline and alkaline earth metals (AEM) on surfaces is of great importance in surface physics and chemistry. This is because the oxidation of these metals plays a very important role in general in many physical processes such as thermionic and photo-emission [1] and thermionic energy conversion [2]. Also alkaline oxides provide surfaces with low work function (WF) and negative electron affinity [3], as well as modifying the catalytic properties of the substrates [4]. Very recently, it has been shown that a BaO thin film on the Si(100) surface, after annealing at 900 K, exhibits WF as small as 0.5 eV [5]. Moreover, AEM oxides contribute a rich variety of physical properties in magnetism, ferroelectricity, structural transformations, metal–insulator transitions and superconductivity [6]. Concerning the latter, the presence of highly ionic cations like Sr and Ba is a necessary requirement for superconductivity in the high-T_c superconducting oxides [7]. The degree of ionicity in alkaline earth oxides (AEO) is of fundamental importance but is still a controversial matter [8–10]. In many applications the AEO exist as ultra-thin films supported on, for example, transition metal surfaces. The interaction

[1] Author to whom any correspondence should be addressed.

of the oxide with the substrate can modify the ionicity (i.e. the extent of covalent bonding between the metal and oxygen). Recently, it was found through *ab initio* calculations that the bonding of BaO on W(100) involves strong hybridization of the W 5d and, intriguingly, the Ba 5d orbitals which are empty in the free atom, thus explaining the large WF decrease [11].

In this work, we present our first experimental results on oxygen and Ba coadsorption on Ni(110) at room temperature. The experimental process of coadsorption was realized by oxygen adsorption on barium pre-covered nickel surfaces. The techniques mainly utilized in this work were Auger electron spectroscopy (AES) and WF measurements.

2. Experimental procedures

All the measurements were carried out in a standard ultra-high vacuum system (UHV) equipped with AES, low energy electron diffraction (LEED), a quadrupole mass spectrometer (QMS), a Kelvin probe for WF measurements, Ar^+ ion sputtering facilities and a heating control system for crystal annealing. The base pressure, in the range of $3–8 \times 10^{-10}$ mbar, was achieved by an ion pump. The substrate was a Ni(110) single crystal with dimensions 1 cm $\times$ 0.5 cm $\times$ 0.1 cm, polished by Metal Crystal and Oxides Ltd. The crystal was attached on an X–Y–Z manipulator. The clean Ni(110) surface presented a sharp (1 $\times$ 1) LEED pattern. A sulfur impurity was removed by argon sputtering, with energy $E = 2$ keV, partial pressure $P_{\mathrm{Ar}} \simeq 5 \times 10^{-5}$ mbar and sputtering time $t \simeq 20$ min. After the sputtering process a carbon impurity was detected and removed by annealing at about 800 K. Ba deposition was done by means of a commercial evaporation source purchased by SAES Getters. Oxygen adsorption took place by supplying molecular oxygen into the experimental chamber through a leak valve. The oxygen purity was 99.998 vol%. The oxygen pressure during dosing was kept constant at about 5×10^{-8} mbar. The oxygen exposure of the surface, l, is expressed in Langmuirs, L (1 L $= 1.3 \times 10^{-6}$ mbar s).

The AES measurements were performed with a primary beam energy $E = 2$ keV. The electrons were collected and analysed by a Varian cylindrical mirror analyser (CMA), with a measured accuracy of 0.1 eV for the O(KLL) peak. The AES signal was recorded in the first derivative mode, $\mathrm{d}N(E)/\mathrm{d}E$, and the intensity was measured from the peak-to-peak height (AP-PH). By convention the energy of the AES peaks was defined at the high energy wing of the differentiated peaks. The WF measurements in the O adsorption experiments were taken continuously at a constant pressure of about 5×10^{-8} mbar. The accuracy of the Kelvin probe signal was 0.02 eV. The Ba coverage on Ni(110) was estimated in monolayers (ML) by combining previous AES, LEED, TDS and WF results [12].

3. Results and discussion

3.1. Ba on Ni(110)

Before starting the coadsorption experiments on Ni(110), it was essential to study (1) Ba and (2) O adsorption on Ni(110). The former was investigated in detail in a previous work [12]. That investigation showed that Ba develops successive homogeneous layers on the substrate, with the first physical layer being equal to 0.75 monolayer (1 ML $= 0.57 \times 10^{15}$ atoms cm^{-2}). At coverage $\Theta \leqslant 1$ ML, Ba adatoms are strongly bound to the surface ($E = 2.9$ eV/atom), while for higher coverage the Ba atoms interact with each other so that the overlayer approaches the properties of metallic Ba. The first layer consists of a mixture of random $c(2 \times 2)$ domains and disordered atoms. Annealing of the substrate enhances the long-range $c(2 \times 2)$ structure, while at the same time 0.35 ML turns into a stable subsurface phase.

3.2. O on Ni(110)

Oxygen adsorption on Ni(110) was also investigated mainly for reference purposes. This adsorption system has been intensively studied in recent decades with a large variety of experimental techniques [13–18]. Although an extensive study of this system is outside the scope of this work, we performed detailed AES, LEED and WF measurements. In figure 1 the AP-PHs of the O($KL_{23}L_{23}$) and Ni($M_{23}M_{45}M_{45}$) transitions are shown versus oxygen exposure, l. In the same figure, the WF variation, $\Delta\Phi$, and some LEED observations are also shown. Similar results have been previously reported by Benndorf *et al* [13]. According to the authors, three different phases of oxygen bonding are observed: (1) chemisorbed oxygen for exposure, $l \leqslant 0.6$–0.8 L, (2) redistributed chemisorbed oxygen atoms with a tendency of incorporation into the substrate for $l \leqslant 5$–10 L and (3) oxygen interacting with nickel atoms, forming NiO islands for $l \geqslant 10$ L. The above-mentioned different oxygen phases are basically characterized by the WF of the surface, Φ, and the O(KLL) signal variation. A close look at figure 1 shows the exposure range of each oxygen phase on Ni(110). The first phase up to $l \simeq 1.3$ L is characterized by a drastic Φ and O(KLL) AES signal increase. The second phase up to $l \simeq 10.5$ L is marked by a slower rate of Φ increase, leading to a broad maximum and also a slower O(KLL) signal increase, ending up in a small plateau. Finally, the third phase takes place at $l > 10.5$ L, with Φ decreasing and the O(KLL) signal increasing. The above description is in very good agreement with Benndorf *et al* [13]. The $\Delta\Phi$ values corresponding to the 2×1 and 3×1 LEED structures are pointed to by arrows in figure 1 at the corresponding exposures. At room temperature only the diffused 2×1 appeared at 0.5 L, while at higher exposures the structure disappeared. At temperature $T \simeq 600$ K, both the 2×1 and 3×1 patterns were sharp, with the former shown up to 21 L. The 2×1 phase has been explained by various models, such as the 'missing-row' [14] and 'added-row' models [16], while the 3×1 is explained by the 'missing-row' [19]. There are arguments in the literature concerning the exact coverage of these phases, which seems to depend on the temperature and preparation process of the substrate.

3.3. Ba and O on Ni(110)

Our next step was the study of the coadsorption of Ba and O on the Ni(110) surface. The procedure we followed was oxygen adsorption on several Ba pre-covered nickel surfaces. In general, the oxygen coverage is assumed proportional to the AES O(KLL) signal. The intensity of this signal is shown in figure 2 for oxygen adsorption on Ba(Θ ML)/Ni(110), where $\Theta = 0$, 0.15, 0.4 and 1.8 ML. The O(KLL) peak grows faster for the bariated surfaces than for the clean one. This implies that the quantity of pre-deposited Ba significantly increases the sticking coefficient of O on the surface. An alternative explanation might be that O on the bariated surfaces gives a stronger O(KLL) signal compared to that of O on the clean Ni, because in the latter case the O atoms are incorporated into the nickel substrate. However, as will be shown later, WF measurements indicate that the O atoms tend to be positioned under the Ba overlayer. Thus, in both cases the O signal is attenuated, which makes the proposition of increased sticking coefficient more likely. An additional indication favouring the Ba-induced increase of the sticking coefficient can be provided by monitoring the O(KLL) AP-PH at very low oxygen exposures ($l \leqslant 1$ L), as figure 3 shows. The initial slopes of the uptake curves for the bariated nickel surfaces are larger than those of O adsorption on the clean Ni. Taking into account that, for the very early stage of O adsorption on Ni (first phase), the O atoms are relaxed at the outermost Ni plane, not resulting in any AES signal attenuation, whereas for O on the bariated surfaces the O(KLL) signal is attenuated, the increase in sticking coefficient is maintained.

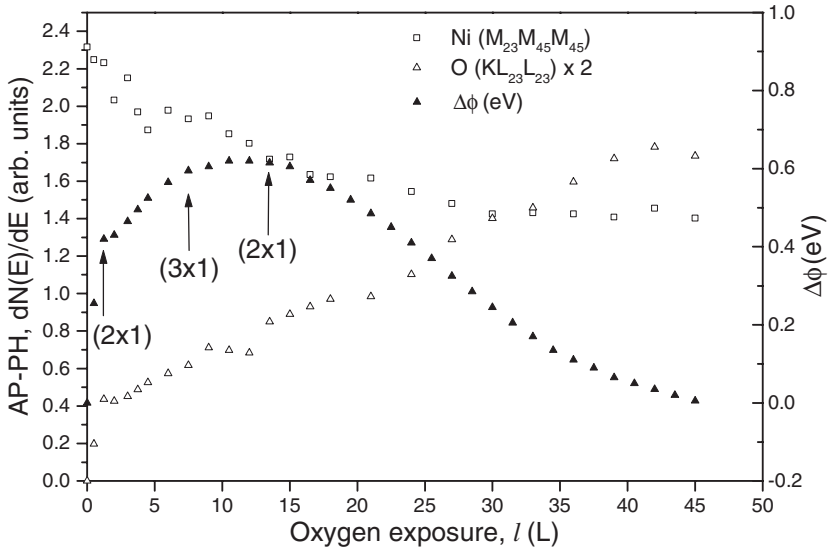

Figure 1. AES and WF measurements for oxygen adsorption on Ni(110). The observed LEED patterns are also marked.

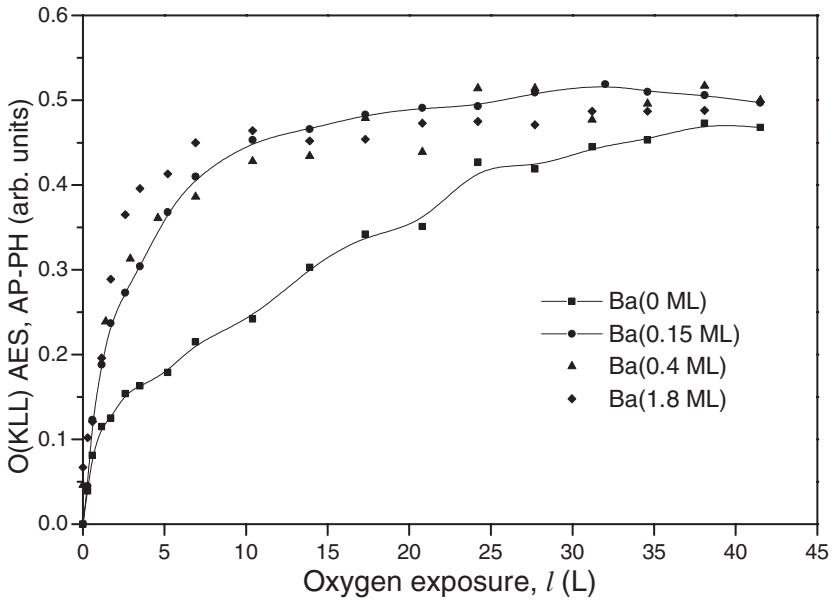

Figure 2. The O(KLL) AP-PH for O adsorption on Ba(Θ ML)/Ni(110), where Θ = 0, 0.15, 0.4 and 1.8 ML. Two guidelines were drawn showing the difference between the clean and the bariated surface.

3.3.1. Analysis of the low energy AES lines. The lineshape of the AES spectra provides important information on the electronic changes taking place on the surface. Figure 4 shows the low energy AES spectra of the (a) O/Ni(110) and (b) O/Ba(0.75 ML)/Ni(110) for several O exposures. For the O/Ni(110) system we observe a decrease and a lineshape change of the

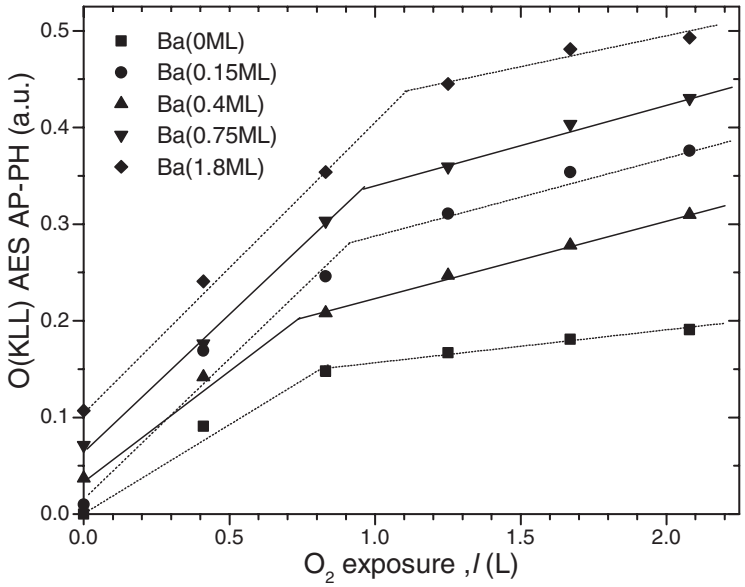

Figure 3. The O(KLL) AP-PH signal for low coverage O adsorption on Ba(Θ ML)/Ni(110), where Θ = 0, 0.15, 0.4, 0.75 and 1.8 ML.

Ni($M_{23}M_{45}M_{45}$) transition at about 61 eV in the course of O exposure. At $l > 10$ L, a relatively weak and broad shoulder, s_1, appears at about 38 eV. At this O exposure, the third phase of the nickel oxidation starts, so s_1 can be associated with NiO island formation. In figure 4(b), a similar shoulder appears in the same energy region at about 35.5 eV. This shoulder differs in energy and shape from s_1 in the O/Ni(110) curves. However, we identify this shoulder with s_1 because these differences are probably due to the different Ni 61 eV pre-peak area between the bariated and the clean nickel surface. We take s_1 as the sign of NiO formation on the surface, which seems to take place on the bariated surface too. A similar AES feature has been observed by Weissmann *et al* [20] and was attributed to an interatomic Auger transition with Ni 3p, O 2s and O 2p atomic orbital participation. It is worth noting that the feature s_1 shows up at oxygen exposures, $1.2 < l < 6.9$ L, for the bariated nickel (figure 4(b)). The appearance of s_1 at a much lower O exposure on the Ba/Ni surface compared to the clean Ni is clearly shown in figure 5. The intensity of s_1 was measured by subtracting from each spectrum of the oxygenated surface that of the non-oxygenated surface. The difference spectra (not shown) in the region of s_1, look more like the standard differentiated AES peak rather than like a shoulder, making possible the AP-PH measurement. The earlier appearance of s_1 in the case of the bariated nickel surfaces suggests that Ba enhances the oxidation of the nickel surface. A plausible explanation for this is the higher sticking coefficient of O on the Ba/Ni surface, already commented on previously. It is worth observing (in figure 5) that NiO development takes place even at relatively high Ba coverage (1.8 ML). This means that a fraction of O atoms incorporate under the Ba layer to react with the substrate. Similar oxygen incorporation happens for O adsorption on cesiated Ni(100) [21].

Ba gives a characteristic AES peak at about 72 eV, which is related to the Ba adatoms on the nickel surface. This peak is denoted by p_1 in figure 4(b) and involves the Ba 4d, 5p and 6s atomic levels. Oxygen adsorption on the bariated nickel causes the appearance of a new AES peak at about 66.5 eV, which is labelled p_2. The p_2 peak evolves at relatively small

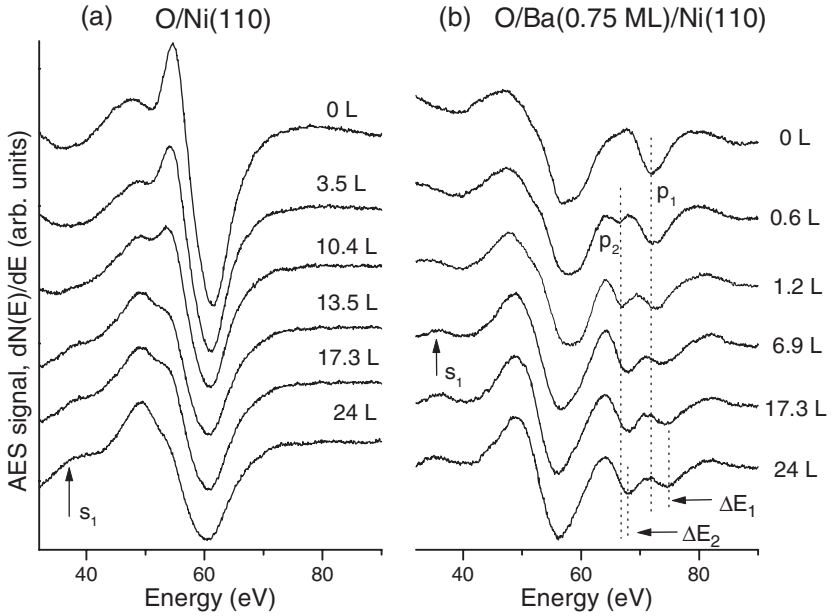

Figure 4. AES spectra of (a) O/Ni(110) and (b) O/Ba(0.75 ML)/Ni(110) for several O exposures.

l ($\simeq$0.6 L), i.e. much earlier than s_1. AES peaks at similar energies have been reported by Haas and Shih [22] in the study of BaO layers on various substrates. More specifically, in the case of W and Nb substrates, the p_2 peak develops at 67.5 eV, whilst for Ir and Rh substrates it is at 69.5 eV. According to the authors, p_2 is due to the Ba–O interaction leading to BaO formation on the surface. The p_2 peak is an interatomic transition involving the Ba 4d, Ba 5p and O 2p atomic levels [23]. The lower energy of this peak with respect to p_1 has been attributed to the valence electron O 2p in the Ba–O system having a lower energy than the 6s in chemisorbed Ba. At the same time this explanation accounts for the differential shift of p_2 for different substrates. When the O atom is weakly bound, as happens on Ir, the final valence state in the AES transition, and hence the Auger electron kinetic energy, is higher than in a more tightly bound state as, for example, on W. In other words, Haas *et al* [22, 23] assumed that the O–substrate interaction plays an important role in the charge transfer between the Ba and O atoms. More specifically, they claimed that the O 2p orbitals fill up not only with Ba 6s but also with the substrate valence band. Nevertheless, they did not find any direct experimental evidence of the O–substrate interaction. In our case the appearance of the s_1 shoulder provides such evidence.

As figure 4(b) shows, the p_2 contribution progressively dominates in the AES spectrum, becoming stronger while the p_1 is weakening. The p_1 peak diminishes, but never disappears. This means that, even at high O coverages, a part of the Ba adatoms have not interacted with O. The intensity variation of the p_1 and p_2 peaks is shown in detail in figures 6(a) and (b), respectively. It is obvious that both the p_1 and p_2 peaks are stabilized in intensity within the exposure range 2.5–5 L. The more Ba is pre-deposited on the surface, the more intense the final p_2 is, i.e. the more Ba adatoms interact with adsorbed O atoms on the surface.

Another important observation in figure 4(b) are the energy shifts ΔE_1 and ΔE_2 for the p_1 and p_2 peaks, respectively, in the course of O exposure. These shifts are displayed in detail in figures 7(a) and (b). To ascertain that the shifts are not artefacts, due to line overlapping,

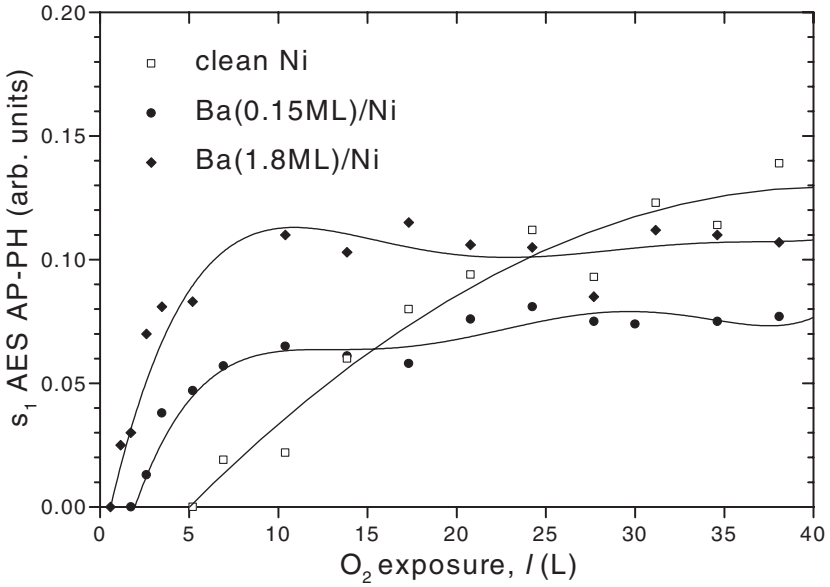

Figure 5. The intensity of the s_1 AES feature versus O exposure on Ba(Θ ML)/Ni(110), where $\Theta = 0$, 0.15 and 1.8 ML.

we simulated each line with the first derivative of a Gaussian, varying the relative heights, widths and peak separation in accord with the original spectra. Examining the sum of the two simulated lines, we did not observe any significant energy shift. We also investigated the possible influence of the intense and broad negative wing of the Ni 61 eV line on the p_1 and p_2 peaks. Again no energy shift was detected. From the above results, we conclude that the energy shifts in figure 7 are real and are probably due to the oxidation process on the surface. This is also supported by the fact that no energy shift was observed for p_1 in the case of Ba adsorption on Ni(110) (not shown). Both the p_1 and p_2 peaks are shifted to higher energy, with an energy change $\Delta E_1 \simeq 3$ eV for the former and $\Delta E_2 \simeq 1.5$–2 eV for the latter. In principle, these positive energy shifts are not what someone would expect. The general trend of AES peaks upon oxidation is a lowering of the measured peak energy [24]. This is to be expected, as the electronegative oxygen atom will remove charge from the neighbouring cation atom, increasing the binding energy (BE) of the remaining electrons. For this reason, the energy shifts ΔE_1 and ΔE_2 for p_1 and p_2 peaks, respectively, need to be clarified.

In general, chemical effects or the influence of the chemical environment of an atom may cause energy changes in AES lines. More specifically, chemical bonding implies a charge transfer, causing a shift of the energy of a core level (chemical shift), which in turn shifts the energy of an AES peak involving this level. The p_2 peak is supposed to be related to the BaO compound formation on the surface, where charge transfer should take place from the Ba to the O atoms due to the ionic character of the bond. The participating O atoms are electronegatively charged, with the O 2p level shifted to lower BE. This might reflect the positive ΔE_2 for p_2. The intense energy change in ΔE_2 is realized in the range 3–6 L (figure 7(b)), where p_2 is almost fully developed (figure 6(b)). In principle BaO is a stable chemical compound which requires an atomic ratio of 1:1 between the Ba and O atoms. At the very early oxygen adsorption stages, this requirement is probably not fulfilled. For this reason we might have, instead of BaO, a precursor state with the Ba–O dipoles interacting

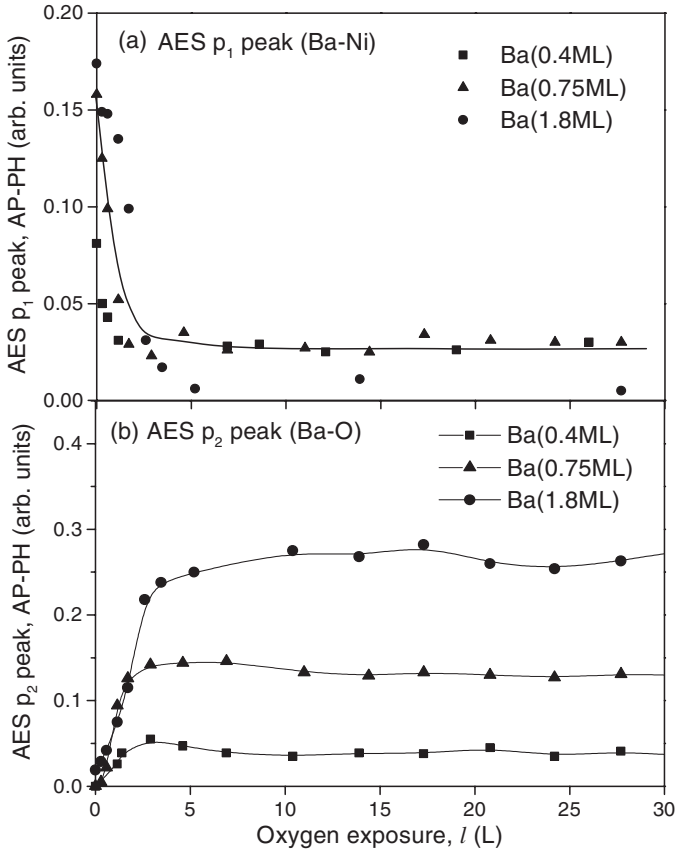

Figure 6. The intensity of the (a) p_1 and (b) p_2 AES peak versus O exposure for Ba(Θ ML)/Ni(110), where $\Theta = 0.4$, 0.75 and 1.8 ML.

with each other. Progressively as the oxygen coverage increases, this precursor state possibly leads to BaO formation, stabilizing the energy of the p_2 peak. An additional factor in the BaO formation delay might be the Ni–O interaction. Indeed, we have observed that NiO formation (the s_1 shoulder in figure 4(b)) starts to take place before the maximization of the p_2 peak, which means that Ba–O and Ni–O interactions coexist and probably compete with each other on the surface.

Another AES peak which might also move to higher energy is the p_1 peak. As was mentioned before, this peak is related to the non-oxidized Ba adatoms on nickel. Haas and Shih [22], while they observed a small energy increase of p_2 for the BaO development on W, they did not record any energy shift for p_1. In our case, however, the recorded ΔE_1 is even bigger than ΔE_2 (figure 7). This means that the Ba adatoms which do not participate in the Ba–O interaction are somehow affected by O adsorption. Although a clear explanation of this influence is not possible from our results, a plausible argument might be related to the effect of local polarization of the Ba atoms due to the field of the Ba–O dipoles.

3.3.2. Analysis of the O(KLL) and Ba(MNN) AES lines. The O(KLL) AES peak at about 510 eV is also shifted in energy. The shift ΔE is shown in figure 8 for O adsorption on Ba(Θ ML)/Ni(110), where $\Theta = 0$, 0.15, 0.4, 0.75 and 1.8 ML. We observe that the final ΔE

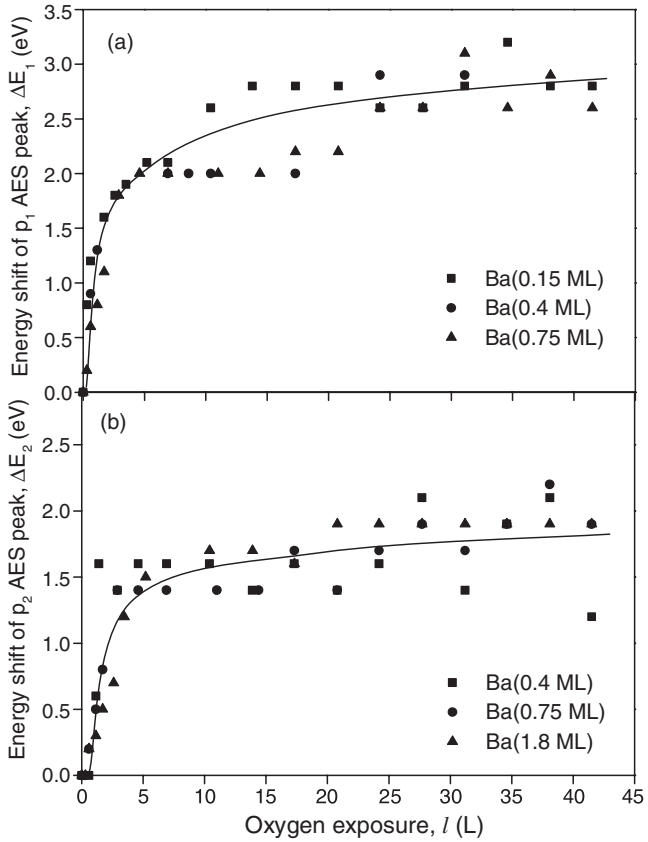

Figure 7. The energy shifts (a) ΔE_1 and (b) ΔE_2 for the p_1 and p_2 AES peaks, respectively, versus O exposure on different bariated Ni(110) surfaces.

depends on the Ba coverage. For the O/Ni(110) system, the peak energy decreases linearly up to $\simeq$23 L and remains stable at $\Delta E \simeq -1.8$ eV. For Ba coverages $\Theta = 0.15$ and 0.4 ML, the energy decreases abruptly up to $\simeq$3 L and stabilizes at $\Delta E \simeq -1$ eV. At $\Theta = 0.75$ and 1.8 ML, O adsorption causes a hardly detectable energy change $\Delta E \simeq -0.15$ eV, which is within the experimental error ($\pm$0.1 eV). The O(KLL) involves core–valence–valence transitions and represents all the adsorbed O atoms, those interacting with Ni as well as those interacting with Ba. The energy shift of the O(KLL) peak to lower energy can be explained by the O 2p moving to higher BE or by the O 1s moving to lower BE. Norton *et al* detected an energy shift of the O 1s level to lower BE ($\simeq$0.8 eV) during the oxidation of Ni(110) [25]. On the other hand, in order to explain the energy shift ΔE_2 of the peak p_2 we have assumed an energy shift of O 2p to lower BE. For $\Theta = 0.15$ and 0.4 ML, where a greater part of the bare nickel surface is exposed to oxygen, it seems reasonable to attribute the initial energy shift to the Ni–O interaction and the chemisorbed O atoms. For $\Theta \geqslant 0.75$ ML, where one or more physical layers of Ba are deposited on nickel, the Ba–O interaction prevails, stabilizing the energy of the O(KLL) peak. It is obvious that more experiments are needed, mostly using x-ray photoelectron spectroscopy (XPS), in order to explain fully all the observed energy shifts of the AES peaks.

The Ba(MNN) double AES peak at about 590 eV was also measured. The peak shows a shift to lower energy by $\Delta E = 1.5$–2.5 eV (not shown), becoming gradually broader after O adsorption.

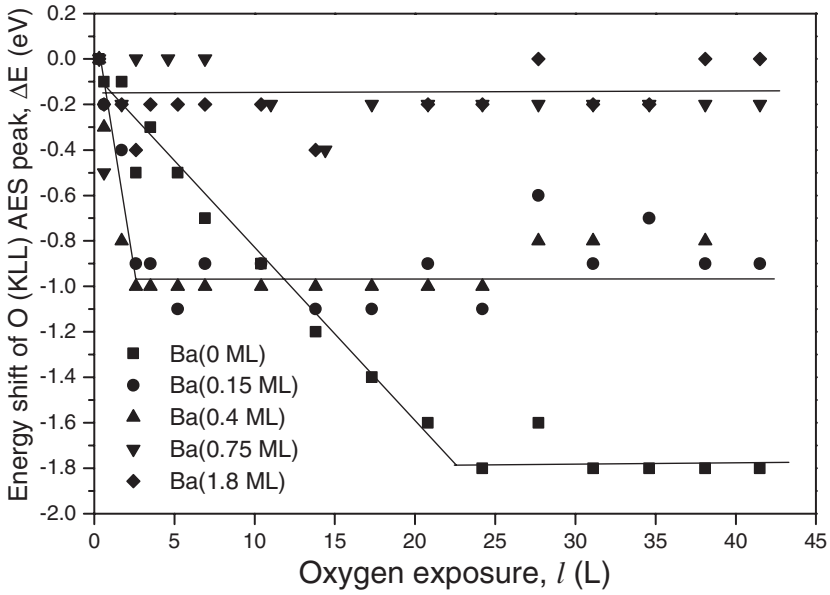

Figure 8. The energy shift ΔE of the O(KLL) AES peak for O adsorption on Ba(Θ ML)/Ni(110), where $\Theta = 0$, 0.15, 0.4, 0.75 and 1.8 ML.

3.3.3. WF measurements. Additional information about the O adsorption mechanism on the Ba/Ni surface can be provided by WF measurements. Figure 9 shows the WF change, $\Delta\Phi$, in the course of O adsorption on the Ba(Θ ML)/Ni(110), where $\Theta = 0$, 0.15, 0.4, 0.75 and 1.8 ML. The diagram is known as a $\Delta\Phi$–Θ–l plot [26], where Φ is the WF, Θ is the metal adsorbate coverage and l is the gas exposure in L. $\Delta\Phi$ is first plotted in the base curve traced by the empty squares as a function of Θ. According to our previous work [12], Ba deposition on Ni(110) causes initially a large Φ reduction up to about 0.45 ML, reaching a WF minimum, $\Phi_{\mathrm{Ba\ min}}$. Further Ba deposition leads to a WF increase to a final value approaching that of the metallic Ba. The added $\Delta\Phi$–l curves, outlined by the filled squares, show the variation of Φ with exposure to oxygen, starting at different coverages of pre-adsorbed Ba. We note that the O adsorption causes an initial Φ decrease down to a minimum Φ_{min}, while further adsorption increases Φ with a tendency to stabilize it. From figure 9, it seems that the larger the value of Θ on the surface, the bigger the initial Φ lowering and the smaller the increase that follows. For $\Theta = 0.75$ and 1.8 ML, Φ decreases with l for up to 3 and 6 L, respectively. Going back to figure 6(b), we see that the p_2 peak is fully developed at about the same l. This coincidence leads us to relate the initial Φ decrease to the BaO development on the surface, with the O atoms probably occupying sites underneath, or at any rate lower, than the Ba adatoms. This is in agreement with the experimental observation that 1 ML of BaO gives lower Φ than 1 ML of Ba on W [27]. Similar behaviour of the $\Delta\Phi$–l curves has been observed for O adsorption on the cesiated MoS_2 surface [28], where the initial Φ decrease was attributed to caesium oxide formation, while the subsequent increase was attributed to O adsorption above the Cs layer. In our case, in contrast to MoS_2, the substrate reacts with O, forming NiO. We can plausibly attribute the Φ increase to NiO development since (a) the NiO Auger feature s_1 still continues to rise after the maximization of the p_2 peak and (b) the WF of this oxide is 4.8 eV [29], much larger than 2 eV of BaO. However, the increase of Φ cannot be explained only by NiO formation, because this increase takes place even after s_1 maximization. An

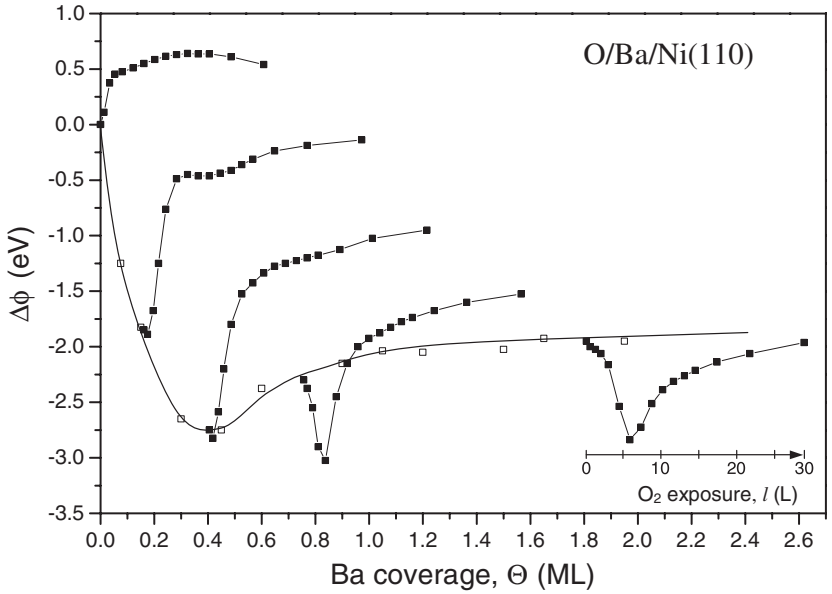

Figure 9. The $\Delta\Phi$–Θ–l diagram for O adsorption on Ba/Ni(110). The $\Delta\Phi$ variation caused by oxygen adsorption is shown by the filled squares, while that with respect to that caused by Ba deposition on Ni(110) is shown by empty squares. Note that the extra x axis, which measures the oxygen exposure, refers to O adsorption on Ba(1.8 ML)/Ni. For the other curves, the zero of this axis should be located at the respective Ba coverages.

additional contribution to this can be due to some of the oxygen atoms occupying sites on top of the pre-deposited Ba adatoms, thus increasing the electric dipole moment towards the surface. This is supported by the small O(KLL) increase after 10 L where the maximization of s_1 and p_2 has occurred.

4. Conclusions

In this work, the O adsorption on bariated Ni(100) surfaces was studied mainly with AES and WF measurements. The following summarizes the major conclusions:

(1) O first interacts with Ba in a precursor state Ba–O, which progressively leads to BaO formation.
(2) O also interacts with Ni forming NiO. Ba pre-deposition enhances nickel oxidation by increasing the sticking coefficient of oxygen on the surface. The O atoms interact with the outermost Ni atoms of the bare substrate or even with those under the Ba layer.
(3) It seems that both Ba–O and Ni–O interactions take place simultaneously, probably competing with each other.
(4) A significant part of the Ba adatoms remains on the surface without reacting with O.

Acknowledgment

DV gratefully acknowledges the Hellenic State Scholarships Foundation, IKY, for financial support during this work.

References

[1] Sommer A H 1968 *Photoemission Materials* (New York: Wiley)
[2] Hatsopoulos G N and Gyftopoulos E P 1979 *Thermionic Energy Conversion* (Cambridge, MA: MIT Press)
[3] Golstein B 1975 *Surf. Sci.* **47** 143
[4] Mross W D 1983 *Catal. Rev. Sci. Eng.* **25** 591
[5] Ikeuchi T, Souda R and Yamamoto S 2002 *Appl. Surf. Sci.* **191** 261
[6] Cohen R E 1992 *Nature* **358** 136
[7] Barr T L and Brundle C R 1992 *Phys. Rev.* B **46** 9199
[8] Pacchioni G, Sousa C, Illas F, Parmigiani F and Bagus P S 1993 *Phys. Rev.* B **48** 11573 and references therein
[9] Pacchioni G and Bagus P S 1994 *Phys. Rev.* B **50** 2576
[10] Pacchioni G and Illas F 1995 *Chem. Phys.* **199** 155
[11] Almanstotter J and Fries T 1999 *J. Appl. Phys.* **86** 325
[12] Vlachos D, Foulias S D, Kennou S, Pappas C and Papageorgopoulos C 1995 *Surf. Sci.* **331–333** 673
[13] Benndorf C, Egert B, Nöbl C, Seidel H and Thieme F 1980 *Surf. Sci.* **92** 636
[14] Smeenk R G, Tromp R M and Saris F W 1981 *Surf. Sci.* **107** 429
[15] Norton P R, Bindner P E and Jackman T E 1986 *Surf. Sci.* **175** 313
[16] Eierdal L, Besenbacher F, Laegsgaard E and Stensgaard I 1994 *Surf. Sci.* **312** 31
[17] Yagi-Watanabe K, Ikeda Y, Ishii Y, Inokuchi T and Fukutani H 2001 *Surf. Sci.* **482–485** 128
[18] Baro A M, Binning G, Rohrer H, Gerber Ch, Stoll E, Baratoff A and Salvan F 1984 *Phys. Rev. Lett.* **52** 1304
[19] Engel T, Rieder K H and Batra I P 1984 *Surf. Sci.* **148** 321
[20] Weissman R, Koschatzky R, Schnellhammer W and Müller K 1977 *Appl. Phys.* **13** 43
[21] Papageorgopoulos C A and Chen J M 1975 *Surf. Sci.* **52** 53
[22] Haas G A and Shih A 1988 *Appl. Surf. Sci.* **31** 239
[23] Haas G A, Marrian C R K and Shih A 1983 *Appl. Surf. Sci.* **16** 125
[24] Briggs D and Seah M P (ed) 1990 *Practical Surface Analysis* 2nd edn, vol 1 (Chichester: Wiley)
[25] Norton P R, Tapping R L and Goodale J W 1977 *Surf. Sci.* **65** 13
[26] Read G E 1991 *Appl. Surf. Sci.* **47** 35
[27] Haas G A, Shih A and Marrian C R K 1983 *Appl. Surf. Sci.* **16** 139
[28] Papageorgopoulos C A 1978 *Surf. Sci.* **75** 17
[29] Papageorgopoulos C A and Chen J M 1975 *Surf. Sci.* **52** 40